Do VLMs Align Better with Humans than LLMs during Natural Reading?

Jinzhou Wu[1,4] **Zhengwu Ma**[2] **Jixing Li**[2] **Baoping Tang**[1] **Zitong Lu**[3*]

[1]Department of Mechanical and Vehicle Engineering, Chongqing University
[2]Department of Linguistics and Translation, City University of Hong Kong
[3]McGovern Institute for Brain Research, Massachusetts Institute of Technology
[4]Sovi.ai, Edgewise Pte Ltd, Singapore

Abstract

Large language models (LLMs) have become increasingly useful computational models of human language processing, but it remains open whether vision-language learning makes text representations more human-like during natural reading. We address this question by comparing matched LLM and vision-language model (VLM) pairs under strictly text-only input and evaluating alignment with human brain activity (whole-cortex fMRI) and human behavior (synchronized regressive saccades). We identify a selective, rather than global, effect of vision–language training on human–model alignment. In the two within-lineage model pairs, VLMs more accurately predicted human regressive saccades, whereas VLMs and LLMs showed comparable whole-cortex fMRI alignment. However, sentence-level analyses revealed that the VLM advantage in fMRI alignment increased with the visual evocative strength of the sentences. Together, these findings provide a controlled in-silico comparison of multimodal training histories, showing that vision-language pretraining selectively improves model–human alignment via reading behavior and visually grounded content.

1 Introduction

Large language models (LLMs) are increasingly used as computational models of human language processing, demonstrating a remarkable capacity for predicting neural activity and behavioral signals during natural reading, story listening, and language comprehension (Schrimpf et al., 2021; Goldstein et al., 2022; AlKhamissi et al., 2025). Consequently, model alignment with human neural and behavioral responses has emerged as an increasingly important benchmark for evaluating whether language models capture human-like language processing (Caucheteux and King, 2022). A truly human-like natural language processing (NLP) model should not only perform well on downstream benchmarks but also mirror the mechanistic ways in which humans process language inputs (Lopez-Cardona et al., 2026; Cichy and Kaiser, 2019; Yin et al., 2025).

However, existing human alignment research has largely focused on pure text representations (Merlin and Toneva, 2024), scaling laws (Gao et al., 2025), next-word prediction objectives (Yu et al., 2024), or instruction tuning (Oota et al., 2025). From an AI perspective, the rapid development of vision-language models (VLMs) raises a natural question for model-human alignment: does multimodal pretraining make language representations more human-like, even when models process text alone? Unlike LLMs trained primarily on text, VLMs are exposed to paired visual and linguistic data, which may encourage representations that capture visually grounded aspects of meaning (Jones et al., 2024). From a cognitive perspective, human language comprehension may also be shaped by multimodal sensorimotor experience, and many concepts are partly grounded in perceptual and action systems (Barsalou, 2010; Binder and Desai, 2011; Lynott et al., 2020). If visual experience contributes to human language processing during reading, VLMs may align more closely than matched LLMs with human neural and behavioral responses (Bavaresco et al., 2025; Xu et al., 2025). This raises the central question of our study: whether and where vision-language learning influences model-human alignment during natural reading. While NLP models cannot be viewed as literal replacements for human subjects (Cichy and Kaiser, 2019), matched LLM/VLM pairs offer a controlled *in silico* system for addressing this question.

Empirical evidence on the comparative brain alignment of multimodal models remains mixed. Concept-word brain alignment can favor VLMs (Bavaresco et al., 2025), whereas comparisons fo-

*Correspondence: Zitong Lu (zitonglu@mit.edu).

cused on experiential semantic information can favor language-only models (Bavaresco and Fernández, 2025). Also, natural-reading work has established neural and eye-movement alignment for language models (Gao et al., 2025; Kuribayashi et al., 2024), and other studies examine online audiovisual movie viewing (Subramaniam et al., 2024; Oota et al., 2025). What remains unclear is not whether models can align with natural reading at all, but whether multimodal training history improves that alignment under text-only inputs, and whether any such effect is whole-cortex, process-level, or content-conditioned. Model-level factors such as architecture, scale, training corpus, and post-training further complicate attribution. A more direct test, therefore, requires matched LLM/VLM pairs with identical text inputs, with these estimands explicitly stated and tested.

In this work, we test how a prior history of vision–language learning is reflected when the same language-only input is processed during natural reading. We first quantify representational differences within matched LLM/VLM pairs, then compare their alignment with regressive saccades and whole-cortex fMRI under identical text-only inputs. We test three estimands: whole-cortex mean alignment, behavioral-level regressive-saccade alignment, and visual-strength-conditioned fMRI alignment. This design turns the broad VLM-versus-LLM question into a controlled and content-resolved comparison rather than a single aggregate brain-alignment score.

Our contributions are as follows:

- We develop an estimand-aware matched-pair framework for comparing LLMs and VLMs. By contrasting text-only language processing in matched model pairs, this framework isolates the contribution of multimodal training history from the effects of online visual input.
- We show that multimodal training reshapes model-internal language representations and improves alignment with human reading behavior, particularly regressive rereading. However, these changes do not translate into a practically meaningful whole-cortex fMRI advantage over matched LLMs during natural reading.
- We introduce a continuous visual strength-moderation analysis of fMRI alignment and reveal that VLMs exhibit stronger brain alignment for visually evocative sentences, and the VLM–LLM alignment difference increases with sentence visual strength. These findings suggest that multimodal training is reflected in human-like language processing in a content-dependent rather than globally brain-like manner.

2 Related Work

Recent studies have increasingly used NLP models as computational probes of human language processing by comparing their internal representations with neural and behavioral responses(Schrimpf et al., 2021; Goldstein et al., 2022; Caucheteux and King, 2022). Transformer-based LLMs can predict fMRI, MEG, ECoG, and eye-movement signals during naturalistic language comprehension, suggesting shared computational structure between language models and the human language system (Tuckute et al., 2024; Antonello et al., 2023; Kuribayashi et al., 2024). Subsequent studies have examined which model properties drive this alignment, including model scale, predictive objectives, associative memory, instruction tuning, and intermediate-layer representations (Aw et al., 2024; Gao et al., 2025). These findings establish model–human alignment as a useful framework for evaluating whether NLP models capture human-like language processing.

A related line of work asks whether multimodal experience makes model representations more human-like. Bavaresco et al. (2025) report stronger VLM brain alignment for concept words in picture or sentence contexts, whereas Bavaresco and Fernández (2025) find language-only models competitive with or superior to VLMs for experiential semantic information and related fMRI alignment. Other studies examine audiovisual or movie settings (Subramaniam et al., 2024; Oota et al., 2025), or sensorimotor and cross-modal concept representations (Xu et al., 2025; Ryskina et al., 2025). These settings differ in input modality, target, and comparison design, leaving open how matched LLM/VLM pairs differ during natural reading of identical text. Detailed comparisons by estimand are given in Table 3 of Appendix A.

Classical embedding-alignment paradigms map sequential hidden states to neural responses (Toneva and Wehbe, 2019). Our fixation-linked BOLD and regressive-saccade targets instead mo-

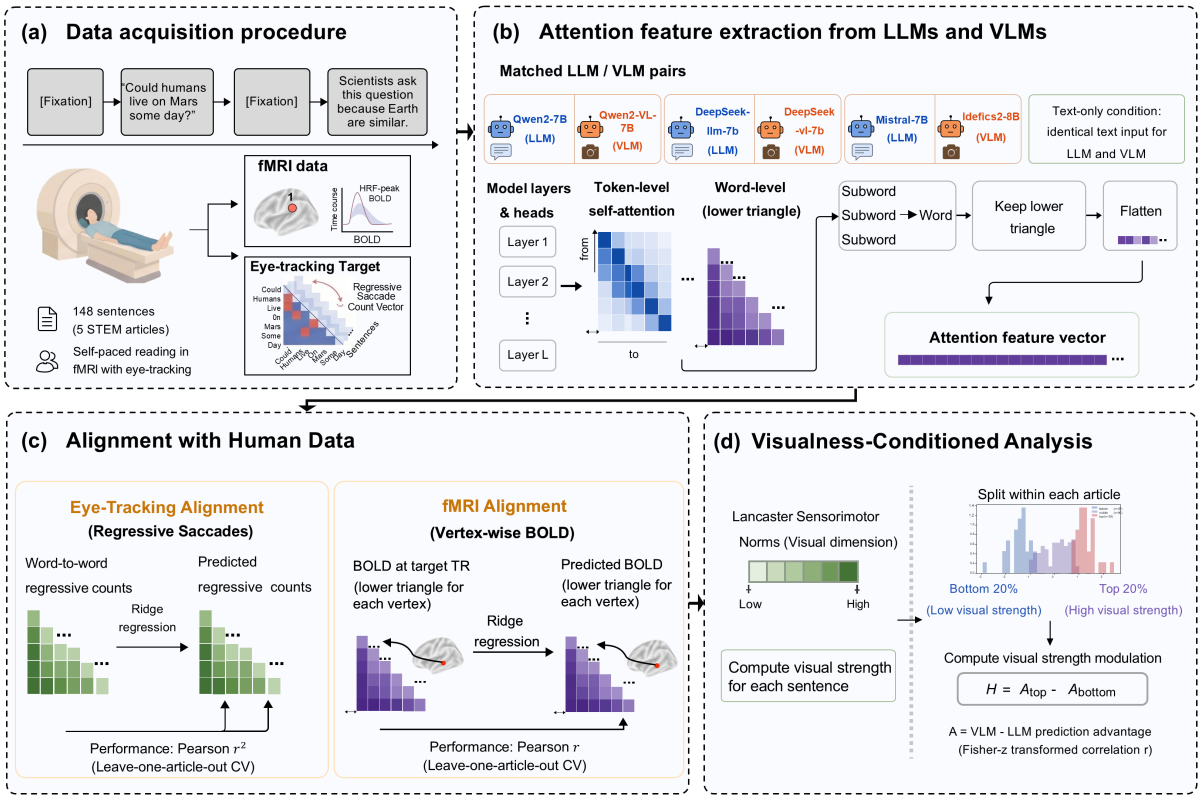

Figure 1: Overview of the matched LLM/VLM alignment pipeline. (a) Data acquisition. Participants read sentences from five articles, one at a time, while concurrent eye-tracking and whole-cortex fMRI are recorded. (b) Attention feature extraction. Layer-wise self-attention matrices are mapped from the token level to the word level, and the lower triangle is retained as the feature representation. (c) Model-human alignment. Lower-triangular attention features are used as predictors in ridge regression models targeting vertex-wise fMRI responses and human regressive saccades during natural reading. (d) A continuous visual-strength-moderation analysis regresses the sentence-level VLM–LLM fMRI-alignment difference on standardised visual strength.

tivate word-pair predictors. We adapt this natural-reading encoding setup to matched LLM/VLM pairs under identical text-only inputs, jointly comparing behavioral alignment, neural alignment, and content-conditioned neural differences for visually evocative text.

3 Methods

We compared matched LLM/VLM pairs under text-only inference and evaluated their alignment with fMRI responses and regressive eye movements during natural reading, illustrated in Figure 1.

3.1 Natural Reading Dataset

We used the openly available Reading Brain dataset on OpenNeuro, which contains eye-tracking and fMRI recordings from 52 adult native English speakers reading naturalistic English texts (Li and Clariana, 2019). Participants read 148 sentences from five English STEM articles, one sentence at a time, inside the scanner, while fMRI and eye movements were recorded concurrently. The data preprocessing details are in Appendix B.

3.2 Matched LLM/VLM Pairs

We evaluated three LLM/VLM pairs at a comparable model scale: (1) Qwen2-7B vs. Qwen2-VL-7B; (2) DeepSeek-LLM-7B vs. DeepSeek-VL-7B; (3) Mistral-7B vs. Idefics2-8B-base. Each VLM uses a language backbone from the same family as its LLM counterpart. In the first-party continued-pretraining pairs (Qwen2, DeepSeek), the VLM is released by the same developer as a multimodal continuation of that exact LLM checkpoint, with text-data lineage continuous across the pair (Yang et al., 2024; Wang et al., 2024; Bi et al., 2024; Lu et al., 2024). Idefics2-8B-base instead initialises from Mistral-7B but is built by a third party around a SigLIP encoder and a Perceiver-style resampler, at a larger parameter count (Jiang et al., 2023; Laurençon et al., 2024). We therefore treat the two in-lineage pairs as the primary comparisons and

Mistral/Idefics2 as a cross-construction robustness case.

All VLMs were run in text-only mode with no image or visual placeholder supplied, so that both models in each pair processed identical textual stimuli. None of these models undergoes instruction tuning. The detailed model configurations are listed in Appendix B.

3.3 Attention Feature Extraction

We follow a fixation-linked natural-reading encoding setup by Gao et al. (2025). Each sentence was passed to each model independently, matching the experimental design in which participants saw one sentence at a time. For every sentence, model layer, and attention head, we extracted token-level self-attention matrices from the language model component. Because the models use subword tokenization, token-level attention was converted to word-level attention using the tokenizer's word IDs. Attention assigned to subword tokens belonging to the same source word was summed across columns, and attention from subword tokens belonging to the same target word was averaged across rows, yielding one word-by-word attention matrix per sentence.

Regressive saccades and fixation-linked BOLD responses are defined on directed word pairs. We therefore retain the strict lower triangle of each word-level matrix, yielding 7,421 shared word-pair entries across sentences. Attention supplies predictors in this space directly, and the contextual-hidden-state control is transformed into the same space. Feature construction details are given in Appendix C.

3.4 Within-Pair Representation Comparisons

We compared word-level hidden-state geometry using RSA and attention distributions using Jensen–Shannon divergence (JSD) on the 148 stimulus sentences. For attention, we report no-sink JSD, which removes sentence-initial attention mass that can dominate raw divergence without reflecting word-to-word patterns. These analyses establish measurable within-pair representational differences under identical text-only inputs. Full definitions, procedures, and attention-sink analyses are provided in Appendix E.

3.5 Eye-movement Alignment

We tested whether model attention predicted human regressive saccades, which reflect rereading and integration of earlier text (Clifton et al., 2007). We therefore tested whether model attention could predict human regressive saccade patterns during sentence reading.

For each matched model pair, the VLM and LLM were compared using a two-sided paired t-test across participants on one participant-level nested-CV alignment score per model. For each outcome, the three prespecified model-pair comparisons were adjusted using the Benjamini–Hochberg procedure. All eye-movement and fMRI encoding analyses used five-fold leave-one-article-out (LOAO) outer cross-validation. Preprocessing, ridge hyperparameter selection, and layer selection were confined to the training portion of each outer fold and the held-out article was used only for final scoring. Encoding details are provided in Appendix C.

3.6 fMRI Alignment

For fMRI alignment, we used the same lower-triangular attention predictors to predict BOLD responses associated with regressive fixation transitions. For each transition, we sampled the BOLD response at the estimated hemodynamic peak, 5 s after fixation onset, and constructed a vertex-wise response vector matched to the same 7,421 word-pair entries. Ridge models were evaluated using the same LOAO encoding procedure, with Pearson's r between predicted and observed BOLD responses as the accuracy metric. Single-model significance was assessed by permutation testing. Matched LLM/VLM pairs were compared using participant-level paired tests on these nested-CV whole-cortex scores. Multiple-comparison correction was applied across the three prespecified model-pair contrasts, and cluster-based permutation testing on the cortical surface (Maris and Oostenveld, 2007). A contextual-hidden-state control using the same targets, CV, and layer-selection policy is reported in Appendix G.

For whole-cortex VLM–LLM contrasts, we distinguish practical equivalence from a nonsignificant result using the TOST against a working ± 0.01 Fisher-z region, and paired BF_{01}.

3.7 visual-strength-conditioned fMRI Analysis

If visual experience selectively shapes the processing of visually grounded language, the VLM–LLM alignment difference may be correlated to how visually evocative a sentence is (Xu et al., 2025).

We therefore tested whether VLMs show a greater fMRI-alignment advantage for more visually evocative sentences.

We defined sentence-level visual strength as the mean Vision rating of matched content words in the Lancaster Sensorimotor Norms (Lynott et al., 2020). We retained 143/148 sentences with at least 75% content-word coverage and at least three matched content words. Visual strength was centred within article before pooled standardisation. For each participant i, cortical unit u, and sentence s, we computed the out-of-fold VLM–LLM alignment difference in Fisher-z space,

$$D_{ius} = z(r_{ius}^{\mathrm{VLM}}) - z(r_{ius}^{\mathrm{LLM}}). \quad (1)$$

We then tested whether this difference increased with visual strength by regressing D_{ius} on sentence visual strength:

$$D_{ius} = \alpha_{iu} + \beta_{iu} V_s + \gamma_{iu} L_s + \delta_{iu,a(s)} + \varepsilon_{ius}, \quad (2)$$

where V_s is the Lancaster visual-strength score standardised across eligible sentences, L_s is effective sentence length, and $\delta_{iu,a(s)}$ denotes article fixed effects. Weights w_s are proportional to the number of eligible directed word-pair observations in sentence s. α_{iu} is an intercept, γ_{iu} captures the length effect, and ε_{ius} is the residual. Therefore, a positive β_{iu} means that the VLM–LLM alignment difference becomes larger as visual strength increases.

To display the relationship at the extremes of the visual strength distribution, we additionally summarized the pattern using grouped visual strength sentences. Within each article, the top and bottom 20% of eligible sentences by visual strength score were labeled high and low visual strength. For each cortical unit u and group $g \in \{\mathrm{high}, \mathrm{low}\}$, we computed

$$A_{u,g} = z(r_{u,g}^{\mathrm{VLM}}) - z(r_{u,g}^{\mathrm{LLM}}), \quad (3)$$

and summarized the extreme-group contrast as

$$H_u = A_{u,\mathrm{high}} - A_{u,\mathrm{low}}. \quad (4)$$

4 Results

4.1 Within-Pair Models Differ in Both Representation Channels

Before interpreting human-alignment contrasts, we quantified how the members of each pair differed under identical text-only inputs. As shown in Table 1, hidden-state RSA was higher for each matched LLM/VLM pair than for the unrelated Qwen2/Mistral reference, but remained below 1.0 in every pair. For attention, Mistral/Idefics2 was the closest pair under both reported descriptive measures: it had the highest RSA and the lowest no-sink attention JSD. These results establish that the released LLM and VLM checkpoints differ in their internal representations, even when the models process identical text-only input.

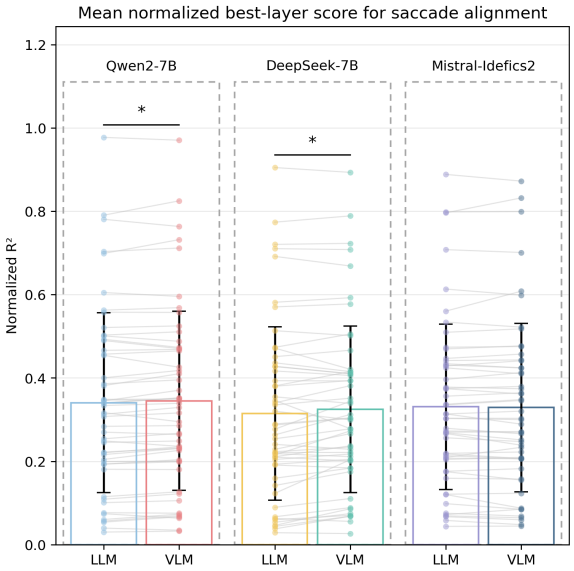

Figure 2: Eye-movement alignment for regressive saccades. Points show subject-level normalized out-of-sample R^2 values. Lines connect the matched LLM and VLM scores for each subject. Asterisks represent significant LLM–VLM differences within a pair on two-sided paired t-tests.

Pair	RSA	JSD (no-sink)
Qwen2 / Qwen2-VL	.897	.0189
DeepSeek / DeepSeek-VL	.810	.0197
Mistral / Idefics2	.952	.0064
Qwen2 / Mistral reference	.574	–

Table 1: Within-pair representation comparisons. RSA is the median hidden-state similarity and no-sink JSD is the median word-level attention divergence with heads retained after removing sentence-initial attention mass.

4.2 VLMs Better Predict Regressive Saccades in the In-lineage Pairs

We then tested whether VLM attention better predicted human regressive eye movements during natural reading. Unlike the global fMRI results, the eye-movement analysis revealed a modest VLM advantage in both first-party continued-pretraining

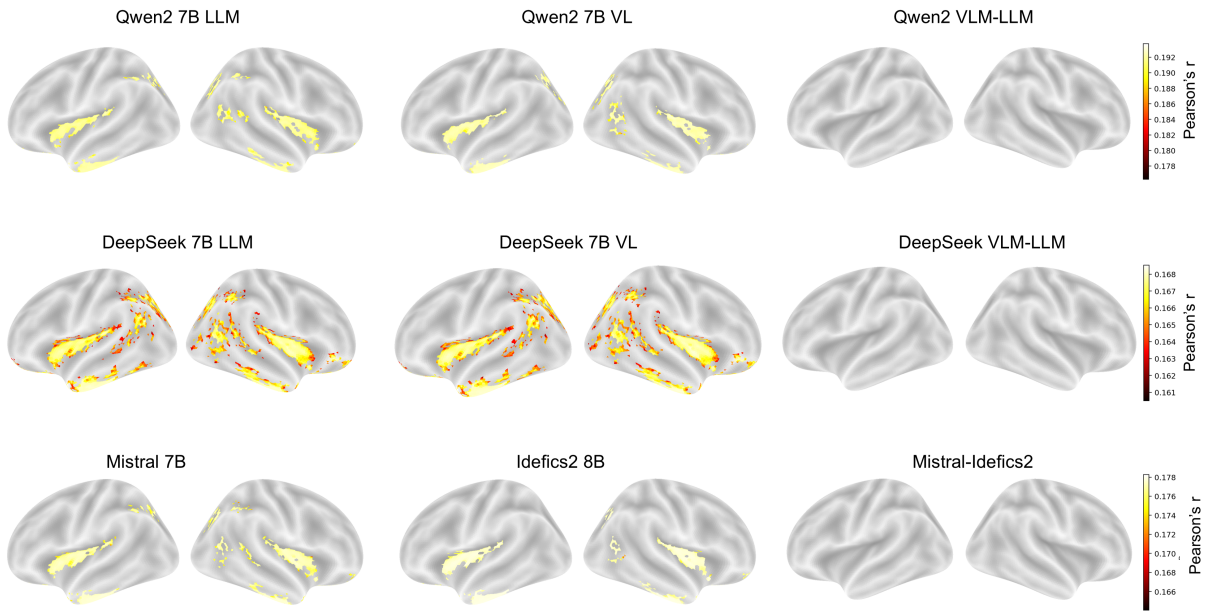

Figure 3: Global fMRI alignment of different LLM–VLM pairs. Significant brain clusters from the single-model-to-brain correlation coefficients and from the contrast of VLM to LLM. Colored regions denote vertex-wise mean effect sizes across subjects. The contrasts are small and do not support a broad whole-cortex fMRI advantage for VLMs during natural reading.

pairs, as shown in Figure 2.

Specifically, Qwen2-VL outperformed Qwen2 in predicting regressive saccade counts under LOAO evaluation (p=.0072). DeepSeek-VL-7B-base likewise outperformed its LLM counterpart (p=.0020). The Mistral/Idefics2 pair did not show evidence of a difference (p=.1711).

This dissociation shows that the whole-cortex fMRI and process-level saccade estimands need not yield the same pattern: the two primary within-family pairs showed higher VLM saccade alignment despite practically equivalent whole-cortex fMRI contrasts. This pattern is consistent with selective, model-pair-dependent differences under text-only input, but does not identify multimodal training history as their causal source. Although Idefics2 uses Mistral as the language backbone, its comparison remains less tightly controlled because tokenizer, training-data, connector, and other architectural differences are confounded across the three pairs.

4.3 Practical Equivalence in Whole-Cortex fMRI Alignment

We then asked whether model attention could predict fMRI responses during text-only natural reading. Both LLMs and VLMs showed reliable fMRI alignment. Surface-based significance maps revealed that individual models predicted BOLD responses in bilateral temporal-parietal regions, including cortical areas commonly associated with language and semantic processing. Thus, model attention captured meaningful variance in neural responses during natural reading, supporting the validity of the alignment framework.

Pair	Δ (95% CI)	BF_{01}	TOST
Qwen2	-0.0006 $[-0.0033, 0.0022]$	6.03	Equiv.
DeepSeek	$+0.0005$ $[-0.0021, 0.0031]$	6.06	Equiv.
Mistral/Idefics2	$+0.0014$ $[-0.0011, 0.0038]$	3.60	Equiv.

Table 2: Whole-cortex fMRI equivalence tests. Attention features were evaluated for all three pairs. Δ denotes the VLM–LLM difference in mean Fisher-z alignment. Equiv. denotes equivalence under TOST with a ± 0.01 Fisher-z bound.

We directly compared each VLM with its matched LLM in Figure 3. Despite robust single-model alignment, whole-cortex VLM–LLM differences were practically equivalent under the working ± 0.01 Fisher-z region (Table 2). A contextual-hidden-state control confirms this pattern: whole-cortex fMRI equivalence holds for all three pairs, and the hidden-state saccade channel reproduces the first-party VLM advantage seen with attention. Detailed description of the hidden-embedding control experiments is in Appendix G.

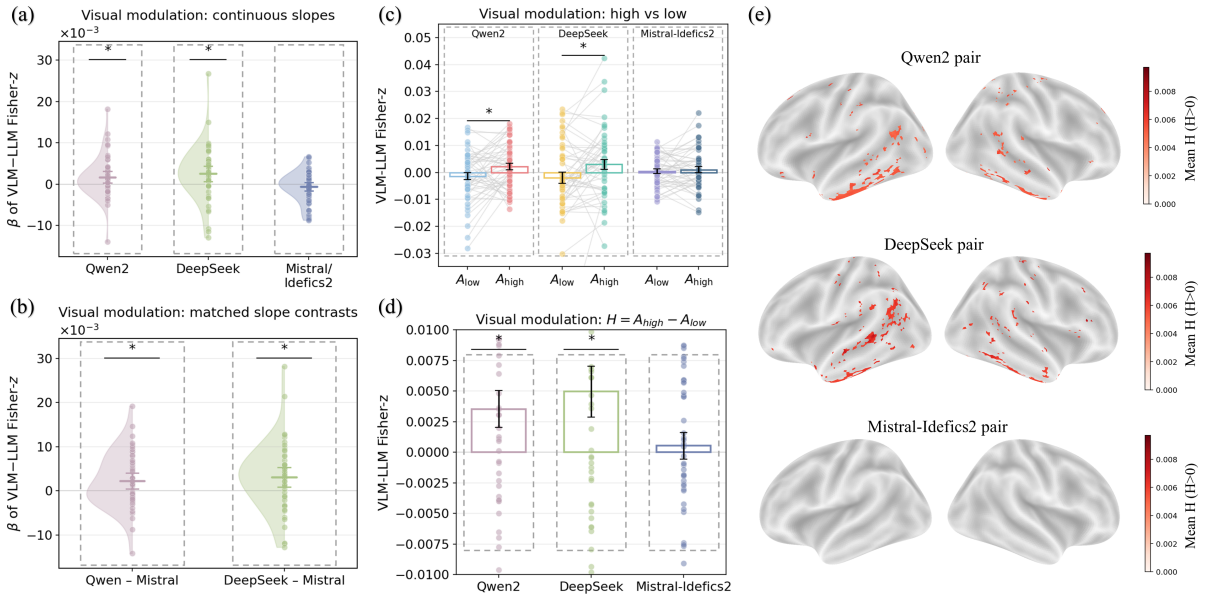

Figure 4: Visual strength modulation of VLM–LLM alignment across matched model pairs. (a) Subject-level whole-cortex continuous moderation slopes β. Each dot is one subject and thick bars denote group means $\pm$ 95% CI. Asterisks denote Holm-corrected one-sided sign-flip $p < .05$ across the three pairs. (b) Within-subject slope contrasts against the cross-architecture stress test (Mistral/Idefics2), Holm-corrected across the two contrasts. (c) Mean advantage in low- and high-visual-strength sentences. Bars denote group means $\pm$ SEM; dots denote individual subjects. (d) Binary modulation index $H = A_{\text{high}} - A_{\text{low}}$ for each pair. Asterisks denote $p < .05$. (e) Cortical localization of the high-vs-low visual strength contrast. Surface projections show vertex-wise mean H within clusters passing a cluster-mass sign-flip permutation test, with cluster-forming $p = .01$, cluster-level $\alpha = .05$ and 10,000 permutations.

4.4 VLM–LLM fMRI Differences Scale with Visual Strength

A whole-cortex mean averages over all sentences and is insensitive to content-dependent effects. We therefore estimated how the VLM–LLM alignment difference scales with sentence-level visual strength.

Both first-party continued-pretraining pairs showed a positive whole-cortex moderation slope that survived Holm correction, as depicted in Figure 4a, indicating that their VLM advantage grew with visual strength. Detailed recordings of visual strength-moderation slopes are in Table 5. The cross-construction Mistral/Idefics2 pair showed no evidence of a visual-strength moderation effect ($p > .05$), similar to the saccade alignment. Participant-matched slope contrasts further showed that both in-lineage pairs had larger slopes than the less tightly controlled cross-construction Mistral/Idefics2 stress test as illustrated in Figure 4b.

The same three-way ordering is visible at the extremes of the visual-strength distribution, as shown in Figure 4c–d, and is preserved under a 25/25 split and under coverage recovery (Appendix D). Exploratory cortical localisation in Figure 4e places the positive moderation effect in clusters including lateral temporal cortex and the angular gyrus, which suggest clustering in bilateral temporal cortex and angular gyrus, regions associated with language and semantic integration (Ivanova et al., 2025; Popham et al., 2021). However, with effects of this size we treat the localization as descriptive.

5 Discussion and Cognitive Implications

The representational analyses establish the model-side basis for the alignment results. Each matched LLM/VLM pair showed measurable changes in hidden-state geometry and attention distributions under identical text-only input, demonstrating that vision-language development leaves a detectable trace in language processing representations. The three pairs also differed in the form of this representational change. The Mistral/Idefics2 stress test was highly similar to its LLM counterpart under both RSA and attention JSD, yet it yielded a non-positive visualness slope and no regressive-saccade advantage. This pattern shows that model–human alignment is shaped by the structure of within-pair representational change, not simply by its descrip-

tive magnitude.

Across the two first-party continued-pretraining pairs, VLMs better predicted regressive saccades, which is reproduced with contextual-hidden-state features (Appendix G). Regressive saccades index rereading and integration during reading (Rayner, 2009). The advantage therefore links vision-language learning to a reading process that supports the construction, integration, and revision of semantic representations.

Whole-cortex fMRI alignment provides the complementary global view. VLMs and their matched LLMs achieved closely matched whole-cortex alignment during natural reading. This global similarity indicates that language-internal distributional, predictive, and compositional representations capture a substantial portion of the neural dynamics engaged during natural reading (Schrimpf et al., 2021; Goldstein et al., 2022). It provides the common computational baseline on which visual-semantic modulation is expressed.

The continuous visual-strength-conditioned analysis identifies this graded structure. Visual-semantic content is especially relevant when sentence meaning evokes objects, scenes, actions, and spatial relations. The positive continuous slopes in the Qwen2 and DeepSeek pairs show that the VLM–LLM alignment difference grows along this graded semantic dimension. The grouped high–low summaries and cortical maps place the convergent pattern in lateral temporal and inferior parietal regions, areas implicated in semantic integration and multimodal conceptual representation (Ivanova et al., 2025; Popham et al., 2021).

Matched LLM/VLM pairs provide a productive computational-experiment framework for cognitive neuroscience. The two first-party pairs retain a shared language lineage, every comparison uses identical text-only input, and the cross-construction pair tests the scope of the pattern under a less tightly controlled configuration. This design makes it possible to connect model-development histories to distinct model–human alignment estimands, including rereading behavior, whole-cortex similarity, and graded visual-semantic modulation.

6 Conclusion

We compared three matched LLM/VLM pairs under text-only inputs during natural reading, jointly testing behavioral alignment, whole-cortex fMRI alignment, and continuous visual-semantic modulation. In both first-party continued-pretraining pairs, VLMs better predicted regressive saccades and showed positive visual-strength-moderation slopes: their fMRI-alignment advantage increased as sentence visual strength increased. Direct participant-matched slope contrasts also separated these pairs from the less tightly controlled Mistral/Idefics2 stress test. Whole-cortex fMRI alignment was closely matched within each pair, revealing a structured profile in which global similarity coexists with process-level and visual-semantic differentiation. These findings establish estimand-aware matched-pair analysis as a route to characterising how vision-language learning shapes model–human alignment during natural reading.

Limitations

The insights discussed in this study are bounded by specific methodological choices that warrant careful consideration in future work. First, although our matched-pair design reduces confounds relative to comparisons between unrelated models, current open LLMs and VLMs do not allow a perfect causal isolation of multimodal pretraining. Model pairs can still differ in training data scale, optimization procedure, multimodal integration design, and other architectural details.

Second, our strictly text-only paradigm intentionally isolates the history of visual learning from online sensory fusion, but it does not capture the dynamic, real-time interactions between language processing and simultaneous visual environments that humans experience daily. The absence of a global VLM advantage during text-only natural reading should therefore not be taken as evidence that visual grounding is irrelevant to language processing more broadly.

Third, our alignment analyses focus on lower-triangular attention features because they provide a natural bridge to regressive eye movements and fixation-linked fMRI responses. This choice makes the neural and behavioral analyses directly comparable, but it does not exhaust all possible model representations that may align with human language processing. In addition, sentence-level visual strength, derived primarily from sensorimotor norms, is only an approximate measure of visually grounded semantic content. Future work should test broader behavioral measures, alternative model features, and richer forms of semantic grounding.

Ethical Considerations

This work aims to analyze the alignment between contemporary models and human language processing during natural reading. Such analyses may contribute to a better scientific understanding of both NLP systems and biological language processing, and may provide a biologically informed perspective on the interpretability and cognitive plausibility of current AI systems (Schrimpf et al., 2021; Gao et al., 2025).

An openly available natural-reading dataset containing fMRI and eye-tracking recordings from adult participants (Li and Clariana, 2019) is used, and no new human-subject data were collected in this study. The original dataset was released for research use, and our analyses were conducted only on the de-identified public data.

Our findings could be interpreted as evidence for the aggregate model—human alignment in a specific natural-reading setting. By clarifying where current language and vision-language models do and do not align with human neural and behavioral responses, we hope this work contributes to the development of AI systems that are more interpretable, cognitively informed, and responsibly integrated into human-centered applications.

References

Badr AlKhamissi, Greta Tuckute, Yingtian Tang, Taha Osama A Binhuraib, Antoine Bosselut, and Martin Schrimpf. 2025. From Language to Cognition: How LLMs Outgrow the Human Language Network. In *Proceedings of the 2025 Conference on Empirical Methods in Natural Language Processing*, pages 24321–24339, Suzhou, China. Association for Computational Linguistics.

Richard Antonello, Aditya Vaidya, and Alexander Huth. 2023. Scaling laws for language encoding models in fMRI. In *Thirty-Seventh Conference on Neural Information Processing Systems*.

Khai Loong Aw, Syrielle Montariol, Badr AlKhamissi, Martin Schrimpf, and Antoine Bosselut. 2024. Instruction-tuning Aligns LLMs to the Human Brain. In *First Conference on Language Modeling*.

Lawrence W. Barsalou. 2010. Grounded Cognition: Past, Present, and Future. *Topics in Cognitive Science*, 2(4):716–724.

Anna Bavaresco and Raquel Fernández. 2025. Experiential Semantic Information and Brain Alignment: Are Multimodal Models Better than Language Models? *Preprint*, arXiv:2504.00942.

Anna Bavaresco, Marianne de Heer Kloots, Sandro Pezzelle, and Raquel Fernández. 2025. Modelling Multimodal Integration in Human Concept Processing with Vision-Language Models. *Preprint*, arXiv:2407.17914.

Xiao Bi, Deli Chen, Guanting Chen, Shanhuang Chen, Damai Dai, Chengqi Deng, Honghui Ding, Kai Dong, Qiushi Du, Zhe Fu, Huazuo Gao, Kaige Gao, Wenjun Gao, Ruiqi Ge, Kang Guan, Daya Guo, Jianzhong Guo, Guangbo Hao, Zhewen Hao, and 67 others. 2024. DeepSeek LLM: Scaling Open-Source Language Models with Longtermism. *Preprint*, arXiv:2401.02954.

Jeffrey R. Binder and Rutvik H. Desai. 2011. The Neurobiology of Semantic Memory. *Trends in Cognitive Sciences*, 15(11):527–536.

Charlotte Caucheteux and Jean-Rémi King. 2022. Brains and algorithms partially converge in natural language processing. *Communications Biology*, 5(1):134.

Radoslaw M. Cichy and Daniel Kaiser. 2019. Deep Neural Networks as Scientific Models. *Trends in Cognitive Sciences*, 23(4):305–317.

Charles Clifton, Adrian Staub, and Keith Rayner. 2007. Eye movements in reading words and sentences. In *Eye Movements*, pages 341–371. Elsevier.

Changjiang Gao, Zhengwu Ma, Jiajun Chen, Ping Li, Shujian Huang, and Jixing Li. 2025. Increasing alignment of large language models with language processing in the human brain. *Nature Computational Science*, 5(11):1080–1090.

Andrew Gelman and Hal Stern. 2006. The difference between "significant" and "not significant" is not itself statistically significant. *The American Statistician*, 60(4):328–331.

Ariel Goldstein, Zaid Zada, Eliav Buchnik, Mariano Schain, Amy Price, Bobbi Aubrey, Samuel A. Nastase, Amir Feder, Dotan Emanuel, Alon Cohen, Aren Jansen, Harshvardhan Gazula, Gina Choe, Aditi Rao, Catherine Kim, Colton Casto, Lora Fanda, Werner Doyle, Daniel Friedman, and 13 others. 2022. Shared computational principles for language processing in humans and deep language models. *Nature Neuroscience*, 25(3):369–380.

Anna A. Ivanova, Carina Kauf, Ruimin Gao, Jingyuan Selena She, Hope H. Kean, Tanya Goldhaber, Alfonso Nieto-Castañón, Rosemary Varley, Nancy Kanwisher, and Evelina Fedorenko. 2025. Semantic reasoning takes place largely outside the language network.

Albert Q. Jiang, Alexandre Sablayrolles, Arthur Mensch, Chris Bamford, Devendra Singh Chaplot, Diego de las Casas, Florian Bressand, Gianna Lengyel, Guillaume Lample, Lucile Saulnier, Lélio Renard Lavaud, Marie-Anne Lachaux, Pierre Stock, Teven Le Scao, Thibaut Lavril, Thomas Wang, Timothée Lacroix,

and William El Sayed. 2023. Mistral 7B. *Preprint*, arXiv:2310.06825.

Cameron R. Jones, Benjamin Bergen, and Sean Trott. 2024. Do Multimodal Large Language Models and Humans Ground Language Similarly? *Computational Linguistics*, 50(4):1415–1440.

Tatsuki Kuribayashi, Yohei Oseki, and Timothy Baldwin. 2024. Psychometric Predictive Power of Large Language Models. In *Findings of the Association for Computational Linguistics: NAACL 2024*, pages 1983–2005, Mexico City, Mexico. Association for Computational Linguistics.

Hugo Laurençon, Léo Tronchon, Matthieu Cord, and Victor Sanh. 2024. What matters when building vision-language models? *Preprint*, arXiv:2405.02246.

Ping Li and Roy B. Clariana. 2019. Reading comprehension in L1 and L2: An integrative approach. *Journal of Neurolinguistics*, 50:94–105.

Angela Lopez-Cardona, Sebastian Idesis, Mireia Masias Bruns, Sergi Abadal, and Ioannis Arapakis. 2026. Brain–Language Model Alignment: Insights into the Platonic Hypothesis and Intermediate-Layer Advantage. In *Proceedings of UniReps: The Third Edition of the Workshop on Unifying Representations in Neural Models*, pages 81–101. PMLR.

Haoyu Lu, Wen Liu, Bo Zhang, Bingxuan Wang, Kai Dong, Bo Liu, Jingxiang Sun, Tongzheng Ren, Zhuoshu Li, Hao Yang, Yaofeng Sun, Chengqi Deng, Hanwei Xu, Zhenda Xie, and Chong Ruan. 2024. DeepSeek-VL: Towards Real-World Vision-Language Understanding. *Preprint*, arXiv:2403.05525.

Dermot Lynott, Louise Connell, Marc Brysbaert, James Brand, and James Carney. 2020. The Lancaster Sensorimotor Norms: Multidimensional measures of perceptual and action strength for 40,000 English words. *Behavior Research Methods*, 52(3):1271–1291.

Eric Maris and Robert Oostenveld. 2007. Nonparametric statistical testing of EEG- and MEG-data. *Journal of Neuroscience Methods*, 164(1):177–190.

Gabriele Merlin and Mariya Toneva. 2024. Language models and brains align due to more than next-word prediction and word-level information. In *Proceedings of the 2024 Conference on Empirical Methods in Natural Language Processing*, pages 18431–18454, Miami, Florida, USA. Association for Computational Linguistics.

Sander Nieuwenhuis, Birte U Forstmann, and Eric-Jan Wagenmakers. 2011. Erroneous analyses of interactions in neuroscience: a problem of significance. *Nature neuroscience*, 14(9):1105–1107.

Subba Reddy Oota, Khushbu Pahwa, Prachi Jindal, Satya Sai Srinath Namburi, Maneesh Singh, Tanmoy Chakraborty, Bapi S. Raju, and Manish Gupta. 2025. Instruction-Tuned Video-Audio Models Elucidate Functional Specialization in the Brain. *Preprint*, arXiv:2506.08277.

Sara F. Popham, Alexander G. Huth, Natalia Y. Bilenko, Fatma Deniz, James S. Gao, Anwar O. Nunez-Elizalde, and Jack L. Gallant. 2021. Visual and linguistic semantic representations are aligned at the border of human visual cortex. *Nature Neuroscience*, 24(11):1628–1636.

Keith Rayner. 2009. Eye movements and attention in reading, scene perception, and visual search. *Quarterly Journal of Experimental Psychology*, 62(8):1457–1506.

Maria Ryskina, Greta Tuckute, Alexander Fung, Ashley Malkin, and Evelina Fedorenko. 2025. Language models align with brain regions that represent concepts across modalities. *Preprint*, arXiv:2508.11536.

Martin Schrimpf, Idan Asher Blank, Greta Tuckute, Carina Kauf, Eghbal A. Hosseini, Nancy Kanwisher, Joshua B. Tenenbaum, and Evelina Fedorenko. 2021. The neural architecture of language: Integrative modeling converges on predictive processing. *Proceedings of the National Academy of Sciences*, 118(45):e2105646118.

Vighnesh Subramaniam, Colin Conwell, Christopher Wang, Gabriel Kreiman, Boris Katz, Ignacio Cases, and Andrei Barbu. 2024. Revealing Vision-Language Integration in the Brain with Multimodal Networks. *Preprint*, arXiv:2406.14481.

Mariya Toneva and Leila Wehbe. 2019. Interpreting and improving natural-language processing (in machines) with natural language-processing (in the brain). In *Proceedings of the 33rd International Conference on Neural Information Processing Systems*, 1339, pages 14954–14964. Curran Associates Inc., Red Hook, NY, USA.

Greta Tuckute, Aalok Sathe, Shashank Srikant, Maya Taliaferro, Mingye Wang, Martin Schrimpf, Kendrick Kay, and Evelina Fedorenko. 2024. Driving and suppressing the human language network using large language models. *Nature Human Behaviour*, 8(3):544–561.

Peng Wang, Shuai Bai, Sinan Tan, Shijie Wang, Zhihao Fan, Jinze Bai, Keqin Chen, Xuejing Liu, Jialin Wang, Wenbin Ge, Yang Fan, Kai Dang, Mengfei Du, Xuancheng Ren, Rui Men, Dayiheng Liu, Chang Zhou, Jingren Zhou, and Junyang Lin. 2024. Qwen2-VL: Enhancing Vision-Language Model's Perception of the World at Any Resolution. *Preprint*, arXiv:2409.12191.

Qihui Xu, Yingying Peng, Samuel A. Nastase, Martin Chodorow, Minghua Wu, and Ping Li. 2025. Large language models without grounding recover non-sensorimotor but not sensorimotor features of human concepts. *Nature Human Behaviour*, 9(9):1871–1886.

An Yang, Baosong Yang, Binyuan Hui, Bo Zheng, Bowen Yu, Chang Zhou, Chengpeng Li, Chengyuan Li, Dayiheng Liu, Fei Huang, Guanting Dong, Haoran Wei, Huan Lin, Jialong Tang, Jialin Wang, Jian Yang, Jianhong Tu, Jianwei Zhang, Jianxin Ma, and 43 others. 2024. Qwen2 Technical Report. *arXiv preprint*.

Congchi Yin, Yongpeng Zhang, Xuyun Wen, and Piji Li. 2025. Improve Language Model and Brain Alignment via Associative Memory. In *Findings of the Association for Computational Linguistics: ACL 2025*, pages 986–999, Vienna, Austria. Association for Computational Linguistics.

Shaoyun Yu, Chanyuan Gu, Kexin Huang, and Ping Li. 2024. Predicting the next sentence (not word) in large language models: What model-brain alignment tells us about discourse comprehension. *Science Advances*, 10(21):eadn7744.

A Comparison of Representative Related Works

Table 3 situates the present study among representative model–human alignment studies. It distinguishes prior work by input setting and the quantity being estimated, because apparent LLM–VLM differences depend on both of these design choices.

B Model and Data Details

B.1 Model Pairing Design

Table 4 summarizes the architecture and pretraining details for the three matched LLM/VLM pairs evaluated in this study. The Qwen2 and DeepSeek pairs share the same model family: the VLM extends its matched LLM with a vision encoder while retaining the language backbone, providing the most controlled within-family comparisons. Idefics2 likewise uses Mistral-7B-v0.1 as its language parent model, but adds a SigLIP vision encoder and Perceiver-style connector and is trained on a distinct multimodal mixture. We therefore treat Mistral/Idefics2 as a backbone-shared but less tightly controlled comparison, not as a fully matched intervention.

All model checkpoints were obtained from Hugging Face. The specific checkpoints used are:

- Qwen2-7B: `https://huggingface.co/Qwen/Qwen2-7B`
- Qwen2-VL-7B: `https://huggingface.co/Qwen/Qwen2-VL-7B`
- DeepSeek-LLM-7B: `https://huggingface.co/deepseek-ai/deepseek-llm-7b-base`
- DeepSeek-VL-7B: `https://huggingface.co/deepseek-ai/deepseek-vl-7b-base`
- Mistral-7B-v0.1: `https://huggingface.co/mistralai/Mistral-7B-v0.1`
- Idefics2-8B-base: `https://huggingface.co/HuggingFaceM4/idefics2-8b-base`

All models are released under permissive open-source licenses. Qwen2/Qwen2-vl, Mistral and Idefics2 are under Apache 2.0. The DeepSeek pair is under MIT license. The Reading Brain dataset is available on OpenNeuro under a CC0 public-domain license. The Lancaster Sensorimotor Norms are publicly available for research use.

B.2 Data Preprocessing

We preprocessed the raw fMRI data from the Reading Brain dataset, following Gao et al. (2025). Preprocessing was conducted using fMRIPrep (v25.0.0) with all default parameters. Volumes exceeding framewise displacement $> .5$ mm or standardized DVARS > 1.5 were flagged as motion outliers. Final resampling to MNI space and the fsaverage5 cortical surface (10,242 vertices per hemisphere) was performed in a single interpolation step using antsApplyTransforms and mri_vol2surf with Lanczos interpolation. The resulting surface time series were stored as GIFTI files. BOLD time series were z-scored within each run. Eye-tracking data were extracted from the events files, which contain fixation onset times and word-level area-of-interest indices. Participant 21 was excluded from eye-tracking analyses due to incomplete recording, and participants 21 and 52 were excluded from fMRI analyses due to preprocessing failures, yielding final samples of 51 and 50 participants, respectively.

C Encoding Model Details

C.1 Predictor Construction and Ridge Regression

Both the eye-movement and fMRI encoding models share the same predictor construction. For each sentence s, layer j, and attention head h, the strict lower triangle of the word-level self-attention matrix $A_{s,j,h} \in \mathbb{R}^{n_s \times n_s}$ (excluding the diagonal) was retained and flattened. These vectors were concatenated across all 148 sentences, producing 7,421 lower-triangular word-pair entries. For each layer j, vectors from all attention heads were stacked to

Study	Input setting	Primary estimand	Main conclusion
Toneva and Wehbe (2019)	Natural text	Sequential embedding–brain mapping	Embedding–brain mapping
Gao et al. (2025)	Natural reading	Fixation-linked attention encoding	Scaling / instruction effects
Bavaresco et al. (2025)	Concept words with picture or sentence context	Concept-word VLM–LLM brain alignment	VLM $>$ LLM
Bavaresco and Fernández (2025)	Concepts and experiential norms	Experiential semantics and fMRI alignment	LLM $\geq$ VLM
Oota et al. (2025)	Video/audio with text	Multimodal instruction-tuned brain alignment	Task-dependent
Ryskina et al. (2025)	Text and concepts	Cross-modal concept consistency	LM–brain alignment; not VLM $>$ LLM
Subramaniam et al. (2024)	Multimodal stories	Online multimodal integration	Multimodal advantage
This work	Text-only natural reading	Whole-cortex, process-level, and visual-strength-conditioned differences	Global equivalence; selective local effects

Table 3: Comparison of representative model–human alignment studies. Conclusions depend jointly on the input setting and the quantity being estimated.

Model	Type	Parameters	Layers	Heads	Pretraining data
Qwen2-7B	LLM	7.6B	28	28 query; 4 KV	$\sim$7T text tokens
Qwen2-VL-7B	VLM	7.6B LLM + 675M vision encoder	28	28 query; 4 KV	Multimodal pretraining uses $\sim$1.4T text/image tokens
DeepSeek-LLM-7B-base	LLM	7B	30	32 query; 32 KV	$\sim$2T text tokens, mainly Chinese and English
DeepSeek-VL-7B-base	VLM	7B language backbone + hybrid visual encoder	30	32 query; 32 KV	VL training uses $\sim$400B vision-language tokens, with language data retained as a major component
Mistral-7B-v0.1	LLM	7B	32	32 query; 8 KV	Not publicly disclosed
Idefics2-8B-base	VLM	8B	32	32 query; 8 KV	VLM pretraining uses $\sim$1.5B images and $\sim$225B text tokens

Table 4: Configurations of the LLMs and VLMs evaluated in this study.

form the predictor matrix

$$X_j \in \mathbb{R}^{7421 \times H_j}, \tag{5}$$

where H_j is the number of attention heads at layer j. Heads were kept as separate predictors because different heads may encode different word-to-word relations. For both modalities, we fit a ridge regression:

$$\widehat{y} = X_j \beta_j + \epsilon, \tag{6}$$

where y denotes either the saccade-count vector $y^{(i)}_{\text{sacc}}$ or the vertex-wise BOLD response vector $y^{(i,v)}_{\text{BOLD}}$. Hidden-state controls replace X_j with PCA-reduced ϕ_{lm} features (128 components fit on the outer training split only).

For the contextual-hidden-state control, h_l and h_m denote mean-pooled subword embeddings for words l and m, respectively. We construct a feature for each directed word pair as

$$\phi_{lm} = [h_l; h_m; h_l - h_m; h_l \odot h_m]. \tag{7}$$

Thus, both the attention and hidden-state channels are evaluated on the same word-pair entries; this construction does not imply that contextual embeddings cannot be used in other alignment formulations.

C.2 fMRI BOLD Response Construction

For each regressive fixation transition from word l to word m with onset time t_{onset} (ms), we sampled the BOLD response at the estimated hemodynamic peak:

$$t_{\text{scan}} = \left\lceil \frac{t_{\text{onset}}/1000 + 5.0}{0.4} \right\rceil, \tag{8}$$

where 5.0 s approximates the hemodynamic peak and 0.4 s is the repetition time (TR). For each participant i, sentence s, and cortical vertex v, we constructed a BOLD transition matrix $B_s^{(i,v)} \in \mathbb{R}^{n_s \times n_s}$, where entry $[l, m]$ contains the BOLD response at vertex v for the fixation transition from word l to word m. The strict lower triangle was concatenated across sentences to obtain $y^{(i,v)}_{\text{BOLD}} \in \mathbb{R}^{7421}$, matching the same 7,421 word-pair entries used as predictors.

C.3 Hyperparameter Selection and Nested Cross-validation

All eye-movement and fMRI encoding analyses used five-fold leave-one-article-out cross-validation, with article identity defining the outer folds. In each outer fold, four articles were used for model selection and fitting, and the remaining article was reserved exclusively for evaluation.

Model layer and ridge regularization strength were treated as hyperparameters and selected jointly within the outer-training data. Specifically, we performed four-fold inner leave-one-article-out cross-validation over the four outer-training articles. For each candidate layer and ridge penalty, the encoding model was fitted on three inner-training articles and evaluated on the remaining inner-validation article. Validation scores were averaged across the four inner folds, and the layer–penalty combination with the highest mean validation performance was selected. The selected configuration was then refitted using all four outer-training articles and evaluated on the held-out outer-test article.

This procedure was repeated for all five outer folds. Predictions from the five held-out articles were concatenated to produce one complete out-of-sample prediction vector for each participant and model. Eye-movement alignment was quantified using the out-of-sample (R^2), whereas fMRI alignment was quantified using the Pearson correlation between predicted and observed BOLD responses at each cortical vertex.

Because layer selection was fully nested within the outer-training data, the primary statistical comparisons were conducted on the resulting participant-level nested-CV scores rather than separately at each model layer. We therefore did not apply a multiple-comparison correction across layers in the primary analysis. For each outcome, the three prespecified LLM–VLM pairwise comparisons were corrected using the Benjamini–Hochberg procedure.

C.4 Statistical Testing

For single-model fMRI significance, a null distribution was obtained at each cortical vertex by permuting the predicted BOLD vector 10,000 times and recomputing the prediction correlation. For matched LLM/VLM comparisons, subject-level vertex-wise r-maps were contrasted using paired tests across participants. Global mean-r comparisons were corrected using Benjamini–Hochberg FDR correction. For cortical surface localization, we used cluster-based permutation testing with 10,000 sign-flip permutations and fsaverage5 surface adjacency (Maris and Oostenveld, 2007), with a cluster-forming threshold of $p = .01$ and cluster-level $\alpha = .05$.

For eye-movement alignment, matched LLM/VLM pairs were compared using paired t-tests across participants on one nested-CV score per participant and model. The resulting p-values were adjusted using the Benjamini–Hochberg procedure across the three prespecified model-pair contrasts.

C.5 Software and Implementation

All analyses were implemented in Python using PyTorch 2.10, MNE 1.61, and SciPy 1.15.3. Attention extraction used Hugging Face Transformers with eager attention implementation enabled.

D Visualness Scoring and Modulation Details

D.1 Visual Strength Distribution

Figure 5 shows the distribution of sentence-level visual strength scores across the Lancaster-scored stimulus sentences used in the moderation analysis.

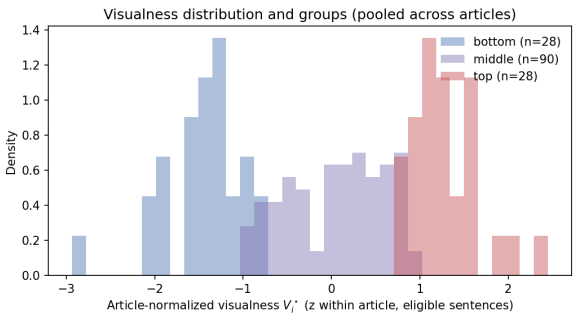

Figure 5: Distribution of sentence-level visual strength scores, computed from the Vision dimension of the Lancaster Sensorimotor Norms. Shaded regions mark the within-article top and bottom 20% used for the extremes summary in Figure 4c–d and Table 6.

D.2 Continuous Moderation Slopes

Table 5 reports the whole-cortex visualness-moderation slopes $\bar{\beta}$ for each matched pair and the participant-matched pair contrasts used to evaluate whether pairs differ. Slopes are estimated from Eq. 2 with sentence length controls, averaged across cortical units within each participant, and tested across participants with one-sided sign-flip

permutation tests (10,000 permutations) and Holm correction across the three within-pair tests.

D.3 Grouped High vs Low Visual Strength Control

To display the moderation at the tails of the visualness distribution, we computed the whole-cortex mean Fisher-z VLM–LLM advantage separately for sentences in the within-article top and bottom 20% of Lancaster visual strength, and report the binary contrast $H = A_{\text{high}} - A_{\text{low}}$ (Table 6). Bayesian evidence (two-sided JZS, Cauchy scale 0.707) favours the alternative for Qwen2 ($\text{BF}_{01} = 0.16$), is ambiguous for DeepSeek ($\text{BF}_{01} = 0.66$), and favours the null for Mistral/Idefics2 ($\text{BF}_{01} = 6.34$). The sign of H agrees with the continuous slope $\bar{\beta}$ for all three pairs.

D.4 Threshold Sensitivity: 25/25 Split

To test sensitivity to the 20/20 grouping threshold, we repeated the extremes summary using a within-article top/bottom 25% split (Table 7). The direction and approximate magnitude of H are unchanged for both first-party pairs.

D.5 LLM-Guided Coverage-Recovery Sensitivity Analysis

The moderation analysis excludes sentences without sufficient Lancaster coverage. To assess sensitivity to that exclusion, we ran a secondary, exploratory coverage-recovery analysis that supplemented low-coverage sentence scores with calibrated estimates from external judges; it does not replace the Lancaster-only analysis.

Of the 148 stimulus sentences, 143 (96.6%) had sufficient Lancaster coverage, four (2.7%) received coverage-recovery estimates, and one (0.7%) was excluded because it contained fewer than three content words. The 3 external judges were outside all evaluated LLM/VLM families. Each judge scored the four low-coverage sentences three times on scene content, visual detail, and imageability (0–5). Scores were calibrated within each LOAO fold against high-coverage Lancaster scores from training articles, then fused by the across-judge median. Prompts, the JSON schema, and decoding settings are provided in the project repository. Algorithm 1 summarizes the procedure. Results are reported in Table 8.

D.5.1 LLM Judge Trigger Rule

For each sentence i, let C_i denote the set of content words and $M_i \subseteq C_i$ the subset matched to entries in the Lancaster Sensorimotor Norms. The norm-based sentence score was defined as

$$V_i^{\text{dict}} = \frac{1}{|M_i|} \sum_{t \in M_i} \text{Vision}(t). \tag{9}$$

Lexical coverage was defined as

$$\kappa_i = \frac{|M_i|}{|C_i|}. \tag{10}$$

A sentence was assigned to the coverage-recovery procedure if $\kappa_i < 0.75$ or $|M_i| < 3$. The resulting sensitivity-analysis score was

$$V_i = \begin{cases} V_i^{\text{dict}}, & \kappa_i \geq 0.75 \text{ and } |M_i| \geq 3, \\ \widehat{V}_i^{\text{LLM}}, & \text{otherwise.} \end{cases} \tag{11}$$

E Representational Change Details

RSA used word-level mean-pooled hidden states and Spearman correlation of correlation-distance RDMs, median across layers, with sentence bootstrap CIs. Unrelated reference: Qwen2 vs. Mistral RSA $= .574$. Attention JSD followed Gao's midpoint implementation of cached word-level attention; per-layer medians were Qwen2 0.0189, DeepSeek 0.0197, and Mistral/Idefics2 0.0064 after sink removal. DeepSeek sink mass (mean attention to word 0 for rows $i \geq 1$) fell from 0.791 to 0.146. Gao instruction-tuning per-layer JSD on the same 148 sentences ranged from 0.0001 to 0.0113. Bootstrap summaries are archived in the project repository.

F Whole-Cortex Equivalence and Sensitivity

For primary whole-cortex contrasts, we report the mean VLM–LLM Fisher-z difference, 95% CI, Cohen's d_z, two-sided paired p, TOST against a working ± 0.01 Fisher-z region, and a paired JZS Bayes factor BF_{01} with Cauchy scale 0.707. We use $\text{BF}_{01} > 3$ as evidence favoring the null relative to the alternative; the equivalence region is not preregistered. We re-evaluated the contrasts under SESOI bounds ± 0.005, ± 0.010, and ± 0.020, and JZS Cauchy scales 0.5, 0.707, and 1.0. Attention- and hidden-channel whole-cortex fMRI decisions remain Equivalent at all three bounds for the reported pairs. At Cauchy $= 0.5$, BF_{01} for attention

Contrast	n	n_+/n_-	$\bar{\beta}$	95% CI	d_z	Holm p
Within-pair slopes						
Qwen2	50	32 / 18	$+.0017$	$[+.0003, +.0031]$	$+0.35$	$.015^*$
DeepSeek	50	34 / 16	$+.0025$	$[+.0006, +.0044]$	$+0.38$	$.011^*$
Mistral/Idefics2	50	24 / 26	$-.0006$	$[-.0016, +.0005]$	-0.16	.857
Participant-matched pair contrasts						
Qwen − Mistral	50	28 / 22	$+.0023$	$[+.0005, +.0040]$	$+0.36$	$.005^*$
DeepSeek − Mistral	50	34 / 16	$+.0031$	$[+.0009, +.0053]$	$+0.40$	$.005^*$

Table 5: Whole-cortex visualness-moderation slopes ($n = 50$). $\bar{\beta}$: mean across cortical units of the regression slope of VLM–LLM Fisher-z difference on standardised Lancaster visual strength, controlling for sentence length (Eq. 2). n_+/n_-: participants with positive/negative slopes. One-sided sign-flip permutation tests (10,000 permutations); Holm correction across three within-pair tests. Pair contrasts are participant-matched $\Delta\bar{\beta}$ values under the same procedure, with Holm correction applied separately across the two pair-contrast tests (Gelman and Stern, 2006; Nieuwenhuis et al., 2011). $^*p < .05$ after Holm correction.

Algorithm 1 External-judge coverage recovery for low-coverage sentences

Require: Sentences $\mathcal{S}$ by article; Lancaster visual norms; judge set $\mathcal{M}$.
Ensure: A fixed sentence-level visual strength table.

```
Define fallback set F = {i : κ_i < 0.75 or |M_i| < 3}.
for all sentences i ∈ F do
    for all judges m ∈ M do
        Query judge m three times using the fixed rubric and JSON schema.
        Obtain scores in [0, 5] for scene content, visual detail, and imageability.
        Average the three sub-scores; take the median across three repeated calls.
    end for
end for
for all leave-one-article-out folds f do
    Let T_f be training articles and H_f the held-out article.
    for all m ∈ M do
        Fit isotonic calibration g_f^(m) using high-coverage sentences in T_f.
    end for
    for all i ∈ F ∩ H_f do
        Set V̂_i^LLM = median_{m∈M} g_f^(m)(q_i^(m)).
    end for
end for
```

Pair	A_L	A_H	H	d_z	BF_{01}	p
Qwen2	$-.0014$	$+.0030$	$+.0043$	0.41	0.16	.003
DeepSeek	$-.0025$	$+.0022$	$+.0047$	0.32	0.66	.013
Mistral/Idefics2	$+.0015$	$+.0014$	$-.0001$	-0.02	6.34	.539

Table 6: Visualness moderation using within-article top/bottom 20% of Lancaster visual strength ($n = 50$). A_{low} and A_{high}: mean Fisher-z VLM–LLM advantages for low- and high-visual-strength sentences. p-values: one-sided sign-flip (10,000 permutations). BF_{01}: two-sided JZS Bayes factor (Cauchy scale 0.707).

Pair	n	H	d_z	Sign-flip p
Qwen2	50	+.003542	0.33	.0113
DeepSeek	50	+.004962	0.34	.0089
Mistral/Idefics2	50	+.000536	0.07	.3147

Table 7: Threshold-sensitivity analysis using a within-article top/bottom 25% split.

Mistral/Idefics2 (2.71) and hidden DeepSeek (2.69) fall slightly below the conventional threshold of 3, so Bayesian evidence should be described as moderate and prior-sensitive rather than uniformly decisive. Full grids are archived with the analysis code.

G Hidden-State Alignment Comparison

To test whether the attention-based conclusions depend on the choice of representation channel, we repeated the fMRI and saccade-count analyses

Pair	n	H	d_z	Sign-flip p
Qwen2	50	+.003634	+0.34	.0099
DeepSeek	50	+.004580	+0.31	.0139
Mistral/Idefics2	50	−.000758	-0.12	.7524

Table 8: Exploratory coverage-recovery sensitivity analysis. The positive direction for Qwen2 and DeepSeek is unchanged relative to the Lancaster-only analysis. Format follows Table 6.

Pair	Δ (95% CI)	d_z	BF_{01}	TOST
Qwen2	$+0.0011$ $[-0.0022, 0.0043]$	$+0.093$	5.29	Equiv.
DeepSeek	-0.0011 $[-0.0032, 0.0009]$	-0.160	3.58	Equiv.
Mistral/Idefics2	-0.0002 $[-0.0020, 0.0017]$	-0.022	6.42	Equiv.

Table 9: Hidden-state whole-cortex fMRI equivalence tests. Format follows Table 2. All three pairs are practically equivalent.

using contextual-hidden-state features ϕ_{lm} under the same nested-CV, LOAO, and the same nested layer–ridge selection procedure.

As for whole-cortex fMRI, Table 9 reports the hidden-state whole-cortex equivalence tests. All three pairs yield practical equivalence under the ± 0.01 Fisher-z working region, converging with the attention-based results in Table 2.

For regressive saccade alignment, Table 10 reports the hidden-state saccade-count results. Both first-party continued-pretraining pairs show a significant VLM advantage, reproducing the attention-based pattern; the cross-construction Mistral/Idefics2 pair does not.

The hidden-state control converges with the attention-based primary analyses on both estimands: no whole-cortex fMRI advantage in any pair, and a selective saccade advantage in the two first-party pairs. The conclusions reported in the main text are therefore not specific to the attention feature channel.

Pair	Δ (95% CI)	d_z	p	Sig.
Qwen2	$+0.0016$ $[0.0002, 0.0029]$	0.333	.021	*
DeepSeek	$+0.0033$ $[0.0019, 0.0047]$	0.646	$<.001$	***
Mistral/Idefics2	$+0.0010$ $[-0.0009, 0.0029]$	0.150	.289	n.s.

Table 10: Hidden-state saccade-count alignment. Both first-party pairs replicate the attention-based VLM advantage (Figure 2), while the cross-construction pair does not.